Journal of Cluster Science (2022) 33:1193–1203
https://doi.org/10.1007/s10876-021-02045-0

ORIGINAL PAPER

Catalytic Activity of Size Tailored Gold Nanoparticles for the Reduction of Environmental Pollutant, 4-Nitrophenol: A Greener Approach

I. V. Asharani[1] · D. Badma Priya[1] · M. Sivagami[1] · D. Thirumalai[2]

Received: 6 October 2020 / Accepted: 9 March 2021 / Published online: 29 March 2021

Abstract

In the present study, we targeted to synthesize size-dependent gold nanoparticles (Au NPs) using aqueous leaves extract of *Actinodaphne madraspatna Bedd* (AMB) both as reducing and stabilizing agents. The different sized Au NPs were effortlessly prepared by varying the concentration of AMB leaves extracts (2%, 3%, 4%). Characterization of synthesized Au NPs was performed by UV–Vis spectroscopy (UV–Vis), scanning electron microscopy (SEM), transmission electron microscopy (TEM), Fourier transform infrared spectroscopy (FT-IR), Brunauer–Emmett–Teller (BET) and X-ray diffraction (XRD). The synthesized Au NPs using different concentrations of AMB leaves extracts were approximately polyhedral in shape as well as the particle size of AmAu2, AmAu3, and AmAu4 nanoparticles were calculated to be 80, 60 as well as 20 nm, respectively. Small-sized particles were obtained with a higher concentration of AMB leaves extract. The potential of the prepared Au NPs as catalyst was assessed by the reduction of organic pollutant 4-nitrophenol (4-NP) to 4-aminophenol (4-AP) using sodium borohydride ($NaBH_4$) as a reducing agent and AmAu4 NPs has exhibited better catalytic activity evidenced by higher rate, when compared with gold NPs reported in the literature. From the study, different sized Au NPs were found to be suitable candidates in the environmental remediation of polluted water.

Keywords Gold nanoparticles · Catalyst · 4-nitrophenol · Kinetics · Size-dependent

Introduction

In recent decades, nanotechnology attracted much attention in the field of science due to synthesis, as well as the development of several nanomaterials. Characteristics of nanoparticles (NPs) differ from the bulk material by their shape and size ranges from 1 to 100 nm. Metal/metal oxide nanoparticles are extensively used in the field of biosensing, catalysis, medicine, imaging, and drug delivery because of their distinctive properties like optical, electrical as well as biological properties [1]. Consequently, it has wide applications in the industrial, medical, agricultural, and environmental fields [2–5]. Nanoparticles have been conventionally synthesized using physical and chemical methods that have enormous negative effects on the surroundings due to toxic chemicals [6–8]. To prevent the agglomeration of nanoparticles due to their smaller size and large surface-volume ratio, a large amount of reducing and capping agents were added in the synthesis [9]. Noble metal nanoparticles have fascinated enormous attention due to its assorted applications in many products especially cosmetics and pharmaceuticals [10]. Among them, gold nanoparticles (Au NPs) gained more consideration mainly because of its catalytic [11, 12], magnetic [13], optical [14], sensing [15], electrical conductivity [16], bio-medical applications [17], anti-microbial activity [18] and Surface-Enhanced Raman Scattering (SERS) [19]. Nowadays, the synthesis of nanoparticles by green method using micro-organism, enzymes, and plants extract augmented ample attention owing to abundance, cheap, and eco-friendly nature [20]. Plants such as *Capsicum annuum, Dalbergia coromandeliana, Sapindus mukorossi Gaertn, Amentotaxus assamica and Mussaenda glabrata* were explored for the synthesis of Au NPs and their catalytic activities also tested [21–25].

4-Nitrophenol (4-NP) is found in the manufacturing as well as agricultural effluents as a pollutant [26–28]. At the

✉ I. V. Asharani
asharani.iv@vit.ac.in

[1] Department of Chemistry, School of Advanced Sciences, VIT, Vellore, Tamil Nadu 63214, India

[2] Department of Chemistry, Thiruvalluvar University, Vellore 632115, India

same time, the formation of 4-aminophenol (4-AP) as a product of 4-NP reduction has enormous applications in the pharmaceutical industry [29]. Authors have already reported the synthesis of silver and palladium nanoparticles using *Actinodaphne madraspatna Bedd* (AMB) leaves extract and assessed their catalytic efficiency towards the reduction of 4-NP [30, 31]. The results were fascinated again to synthesis size-dependent Au NPs using AMB leaves extract simply by varying the concentration of the AMB leaves extract and investigating catalytic efficiency towards reducing 4-NP.

Materials and Methods

Tetrachloro auric(III) acid ($HAuCl_4{\cdot}3H_2O$) and 4-nitrophenol (4-NP) were procured from SRL, India. Sodium borohydride ($NaBH_4$) was bought from Merck, India. All analytical delivered grade chemicals were used as such. The leaves of *Actinodaphne madraspatna* Bedd were gathered as a green reducing agent from Talakona forest, Tirupathi, South India.

Green Synthesis of Au NPs Using *Actinodaphne Madraspatna Bedd* Leaves

To study the effect of concentration of AMB leaves extract in the synthesize of size tuned nanoparticles, 4 mL of 1 mM aqueous $HAuCl_4{\cdot}3H_2O$ was added separately to various concentrations [1 to 5% (w/v)] of AMB leaves extract. The mixture was stirred for 15 min at room temperature at 400 rpm, which turned to pink color finally, showed the development of Au NPs. In the same way, the influence of the concentration of $HAuCl_4$ as well as pH for the synthesis of Au NPs were also investigated.

Characterization of Gold Nanoparticles (Au NPs)

The prepared Au NPs were well characterized by a UV–Vis spectrophotometer (Jasco-V670). The TEM (JEOL JEM) was performed to confirm the size and morphology of the nanoparticles. The selected diffraction ring patterns (SAED) and also lattice fringes were obtained using high-resolution mode. The X-ray Diffraction (XRD, BRUKER D8) analyzer with CuKα radiation (λ = 1.5406) was used to analyze the crystalline phases of Au NPs. The Brunauer–Emmett–Teller (BET) specific surface area of Au NPs was measured by adsorption–desorption study of nitrogen molecules at 77 K using a Quanta chrome Nova 1000 analyzer.

Catalytic Reduction of 4-Nitrophenol

The UV–Visible spectrophotometer was used to evaluate the catalytic reduction of 4-NP in the presence of Au NPs along with aqueous $NaBH_4$ as a catalyst and reducing agent respectively in a quartz cuvette. Similarly, the influence of catalyst load, concentration of $NaBH_4$, and concentration of 4-NP to the catalytic reduction have also been performed. The kinetic studies showed that the found results match with the pseudo-first-order rate equation; hence the rate constant 'k' values were calculated accordingly.

Results and Discussion

Optimization of Size Tuned Green Synthesized Au NPs

The development of Au NPs was followed by UV–Vis spectrophotometer by the Surface Plasmon Resonance (SPR) peak of the nanoparticles and its optimization parameters were listed in Table S1. Figure 1a exhibited the UV–Vis spectra of the synthesized Au NPs using different concentrations of AMB leaves extract (1, 2, 3, 4, and 5%) in the presence of 1 mM $HAuCl_4{\cdot}3H_2O$. The SPR band was gradually shifted from 558 to 530 nm when the concentration of AMB leaves extract increased from 1 to 4%, but beyond 5% significant shift in the SPR band was not observed. So, 4% of AMB leaves extract was preferred as an optimum concentration to study the concentration effect of $HAuCl_4{\cdot}3H_2O$ and pH, during the preparation of Au NPs. Similarly, the effect of concentration of $HAuCl_4{\cdot}3H_2O$ (0.2 to 1 mM) was examined by keeping the concentration of AMB leaves extract as 4% during Au NPs synthesis (Fig. 1b). The peak intensity at 530 nm was continually increasing by increasing the $HAuCl_4{\cdot}3H_2O$ concentration, which showed that the formation Au NPs increases with increasing the $HAuCl_4.3H_2O$ concentration. This may be due to the availability of a large number of gold nuclei when $HAuCl_4{\cdot}3H_2O$ concentration was high. Similarly, the effect of pH was studied during the green synthesis of Au NPs by changing the pH from 3 to 12 in presence of 4% AMB leaves extract as well as 1 mM $HAuCl_4{\cdot}3H_2O$ (Fig. 1c). But characteristic shift or noticeable increase in intensity was not noticed at 530 nm. The overall results indicated that the size of Au NPs varies by different concentrations of AMB leaves; thus, by optimizing the parameters, desired particle size could be tuned, which was tabulated in Table S1. Figure 1d indicate the formation AmAu2, AmAu3 and AmAu4 in the presence of 2, 3 and 4% concentrations of AMB leaves extracts respectively.

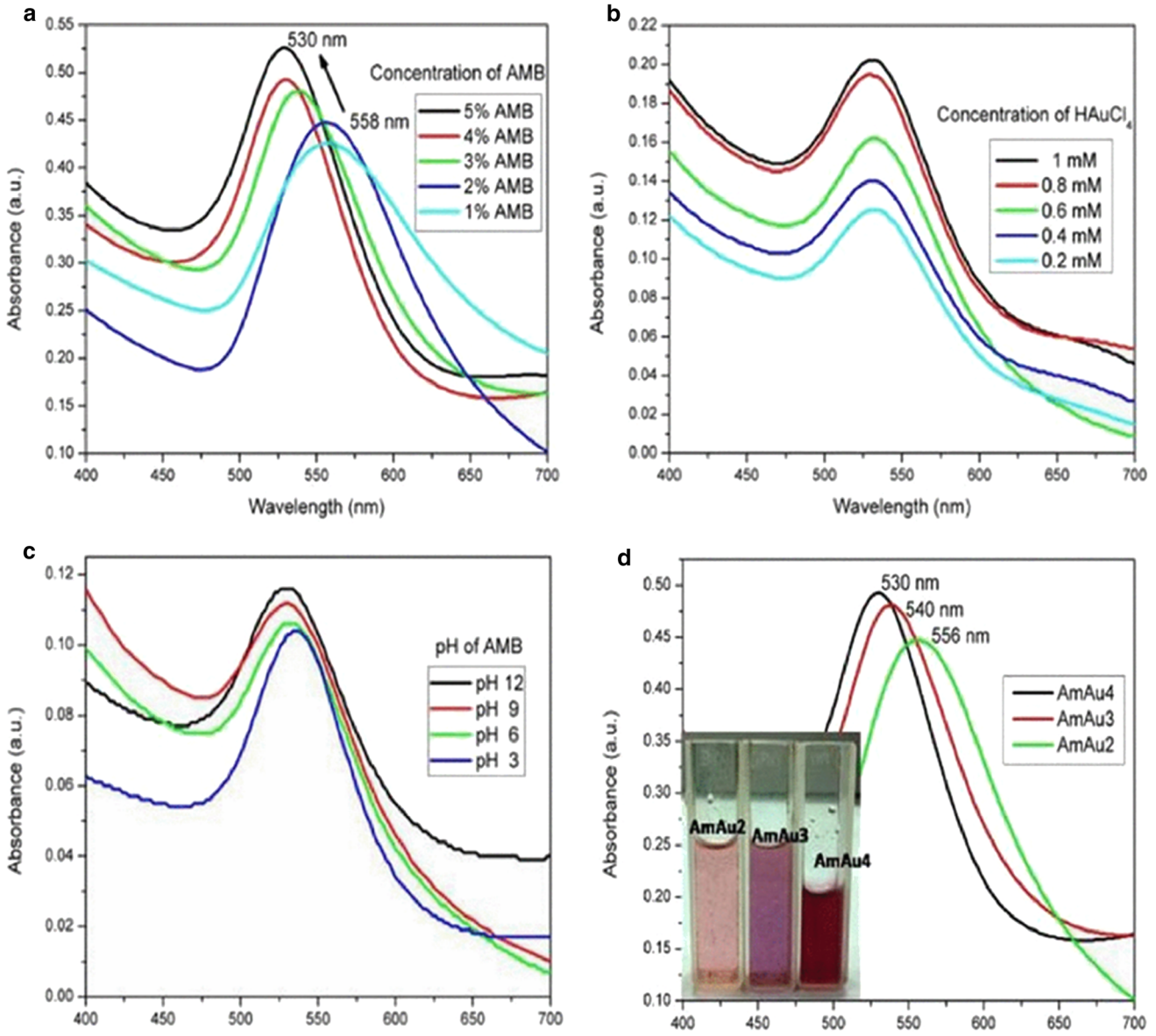

Fig. 1 UV–Vis spectra of the synthesized Au NPs at **a** various concentrations of AMB leaves extract with 1 mM $HAuCl_4{\cdot}3H_2O$. **b** various concentrations of $HAuCl_4{\cdot}3H_2O$ with 4% AMB leaves extract. **c** 4% AMB leaves extract with 1 mM $HAuCl_4{\cdot}3H_2O$ under different pH. **d** prepared Au NPs using various concentrations of AMB leaves extract: 2% (AmAu2), 3% (AmAu3) and 4% (AmAu4) with 1 mM $HAuCl_4{\cdot}3H_2O$

Characterization of the Synthesized Au NPs

TEM analysis was used to investigate the size, morphology, and crystalline nature of the prepared AuNPs. Figure 2 indicated that the prepared AuNPs at various concentrations of AMB leaves extracts were polyhedral in shape and crystalline in nature, which was indicated by the appearance of bright spots in the concentric diffraction rings showed by the selected area electron diffraction (SAED) pattern. The particle size of AmAu2, AmAu3, and AmAu4 nanoparticles was calculated to be 80, 60 as well as 20 nm, respectively. The particle size was observed to be decreased by increasing the concentration of AMB leaves extract and the results were in agreement through the blue shift in the SPR bands acquired from the UV–Vis spectra [32, 33].

Moreover, XRD analysis revealed the crystalline nature of the green synthesized Au NPs. The prepared Au NPs (Fig. 3a) showed diffraction peaks at 38.1°, 43.1°, 66.5°, and 77.7° corresponded to (111), (200), (220), and (311) of face center cubic (fcc) lattice which is based on JCPDS file No: 04-0784 [33, 34]. The crystalline size of the gold nanoparticles was calculated using Scherrer equation and the crystalline size are 27.37, 21.15 and 12.33 nm for

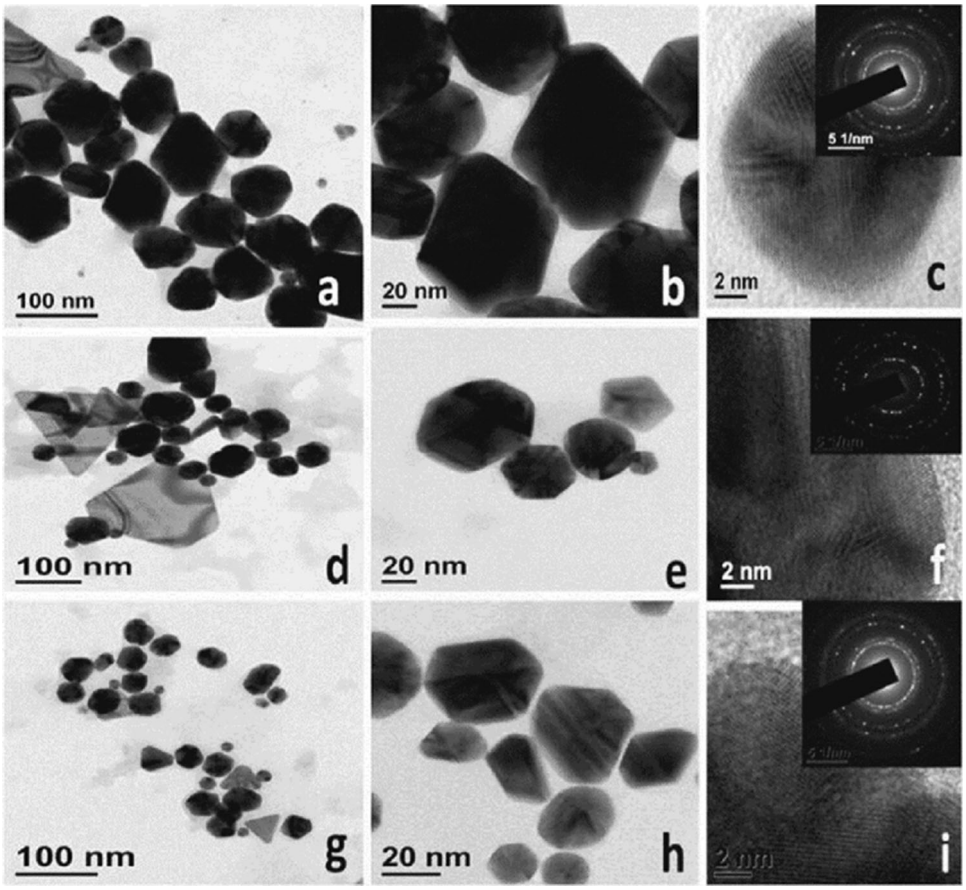

Fig. 2 TEM Images of **a**–**c** AmAu2, **d**–**f** AmAu3 and **g**–**i** AmAu4 Nanoparticles. (Inset showing the corresponding SAED Pattern)

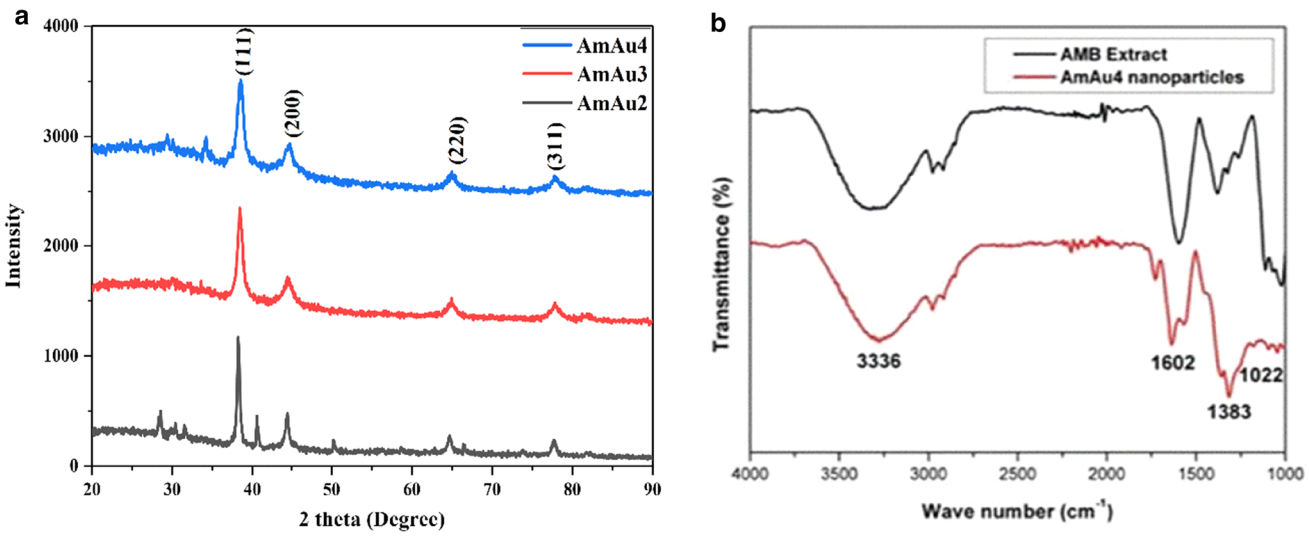

Fig. 3 **a** XRD pattern of synthesized AmAu4, AmAu3 and AmAu2 NPs and **b** FTIR Spectra of AMB Leaves extract as well as AmAu4 NPs

AmAu2, AmAu3 and AmAu4 NPs, respectively based on the highest intense (111) plane.

The phytomoieties present in AMB leaves extract played a vital role throughout the synthesis of Au NPs which was shown by FTIR spectroscopy. IR spectrum of AMB leaves extract with important peaks at 3336, 1602, 1383, and 1022 cm^{-1} were shown in Fig. 3b. These major peaks were attributed to saponin, triterpenoids, flavonoids, steroids, glycosides tannins, alkaloids, as well as carbohydrate compounds of AMB, leaves extract which was in good agreement with the previous reports [35–37]. The new peak at 1643 cm^{-1} (Fig. 3b) might be attributed to the

stretching vibration of the carbonyl group that formed during the reduction process of AmAu4 NPs. Therefore, during the formation of Au NPs, it was expected that phyto-moieties of AMB leaves extract with functional group –OH was oxidized to aldehydes/ketones. Additionally, the FTIR spectrum of AmAu4 NPs (Fig. 3b) exhibited substantial variations in the position as well as the intensity of the functional peaks (flavonoids/polyphenols) of AMB leaves extract that was shown the participation of its phyto-moieties throughout the synthesis of Au NPs as capping as well as stabilizing agents. The minor change in the peak positions may be due to the π-electrons existing in the aromatic phyto-moieties of AMB leaves extract shifted to the free orbital of Au ions through the Red/Ox route as well as reduced to Au0 NPs [38]. The results obtained from FTIR spectra were comparable with previously reported plant assisted Au NPs [39, 40]. The probable mechanism for the formation of Au NPs is given in Fig. 4.

The zeta potential measurements (Fig. 5) were performed to find out the stability of synthesized Au NPs, listed in Table S2. The AmAu4 NPs having high surface-to-volume ratio due to smaller particle size tends to gather extra negative charges of the oxidized form of phyto-moieties of AMB leaves extract covered on the AmAu4 NPs surface which resulted in slightly higher zeta potential values compared to AmAu3 and AmAu2 NPs, thereby reducing the chances of agglomeration between the nanoparticles [41].

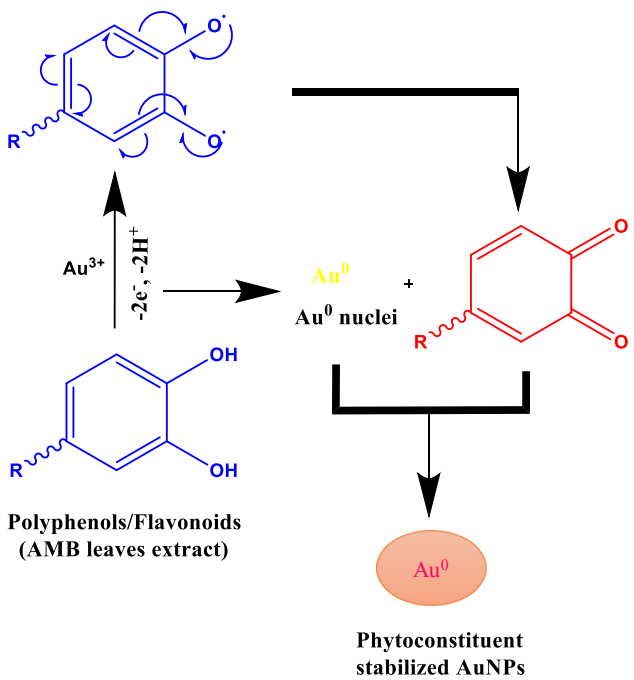

Fig. 4 Probable mechanism for the formation of Au NPs using AMB leaves extract

The BET gas adsorption method is used for the determination of the surface area of the gold nanoparticles. Figure 6 shows the BET plots of the gold nanoparticles prepared in the TritonX-100 based microemulsions at different concentrations of the AMB leaves extract. The specific surface area of the gold nanoparticles increases from 10.8 to 25.6 m^2/g as the concentration of the leaves extract decreases from 4 to 2%. As can be seen, the particle size decreases from 27.3 to 12.3 nm as the leaves concentration of the AMB regularly increases from 2 to 4% [42–44].

Based on the data obtained, it was suggested that the Au NPs with three-different sizes could be easily prepared by changing the concentration of AMB leaves extract. The phytoconstituents that exist in the AMB leaves extract played a dual role in reducing and protecting agents during the Au NPs formation. Therefore, we have proposed a plausible correlation of Au NPs of different sizes under different AMB leaves extract concentration with its size and zeta potential values (Fig. S1).

Catalytic Activity of Synthesized Au NPs

The catalytic efficiency of the prepared Au NPs has been examined towards the reduction of 4-nitrophenol to 4-aminophenol. The kinetics of the reduction reaction was studied using an UV–Visible spectrophotometer in the presence of Au NPs (catalyst) as well as $NaBH_4$ (reducing agent). The peak of 4-NP was shifted from 317 to 400 nm owing to 4-nitrophenolate ion (Fig. 7a) formation upon before $NaBH_4$ addition to the reaction medium. This peak remains unaltered even an hour indicated that the reduction reaction proceeds only in the presence of a catalyst [45]. Therefore, 7 µL of Au NPs was added to the reaction mixture with 4-NP (0.1 mM) and excess of $NaBH_4$. As a result, a steady decrease in intensity at 400 nm was observed, indicating the reduction reaction occurred significantly in the presence of Au NPs catalyst (Fig. 7b) [46, 47].

The rates of the reduction reaction were found to be independent of $NaBH_4$ concentration since its concentration was considerably higher than that of 4-NP, and hence the reaction follows pseudo-first-order for 4-NP. The effect of different key parameters like 4-NP concentration, catalyst dosage as well as $NaBH_4$ concentration on 4-NP reduction was also thoroughly examined.

The Effect of Catalyst Dosage

To examine the influence of synthesized Au NPs as nanocatalyst on the reduction of 4-NP, the reduction reaction was performed with different dosage (4 to 12 µL) of Au NPs whereas other parameters like 4-NP

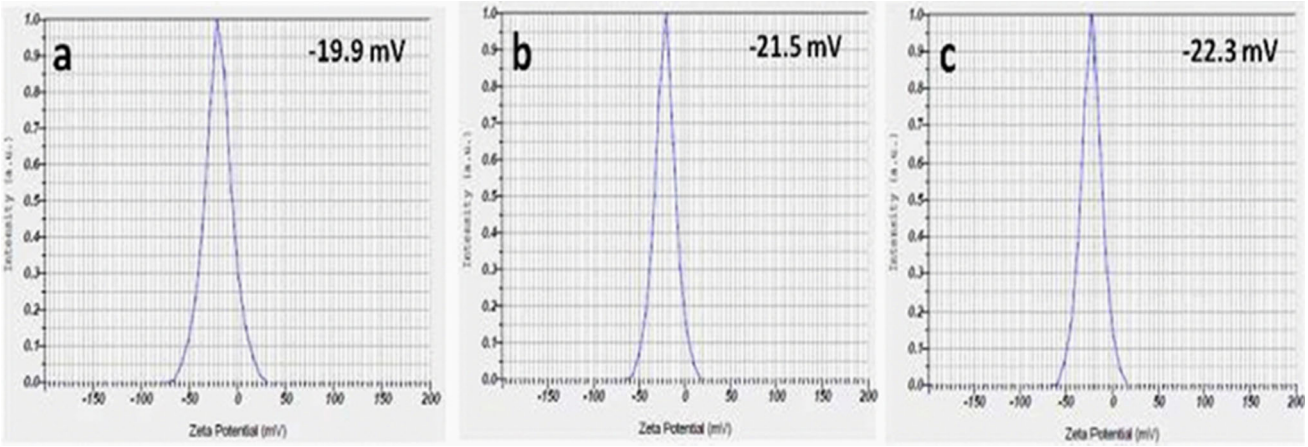

Fig. 5 Zeta potential of prepared **a** AmAu2, **b** AmAu3 and **c** AmAu4 NPs

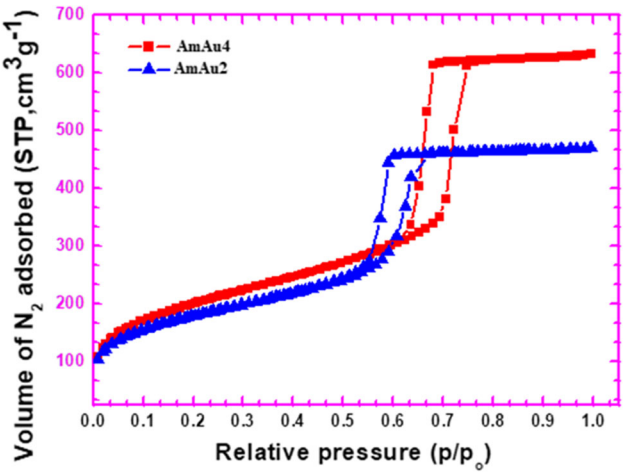

Fig. 6 BET analysis of synthesised Au NPs

concentration (0.1 mM) as well as $NaBH_4$ (5 mM) were kept constant. The absorbance values of 4-NP decrease with time was observed during the reduction of 4-NP. Based on the absorbance values, ln (A_t/A_0) vs time 't' was plotted for different Au NPs dosages, presented in Fig. 8a besides rate constant 'k' values were measured from the concern slope. Here, 'k' values of the reduction reaction were observed to be increases with an increase in Au NPs dosage (Fig. 8b) besides showed in Table S3. The larger amount of Au NPs (12 µL) provides a higher number of nanoparticles to reaction medium with excess surface-to-volume ratio with a lot of active sites available for the reactants (4-NP and BH_4^-) to adsorb simply on the nanocatalyst surface followed by the rapid relay of electron among BH_4^- as well as 4-NP. Thus, 4-NP reduction occurred faster with higher rate constant 'k'. On the other hand, the rate constant 'k' was found to be lesser with lower dosage of Au NPs (4 µL), owing to the reduced number of available nanoparticles for reactants to adsorb and this may produce a competition among reactants on the catalyst surface, which hindered the reaction hence results in low reduction rate.

The Effect of Concentration of 4-NP

It was our interest to find out the influence of 4-NP concentration (0.050 to 0.125 mM) on reduction reaction, $NaBH_4$ (5 mM) concentration as well as Au NPs (7 µL) were kept constant. Figure 9a represents the plot of ln (A_t/A_0) vs time 't' of the reduction of various concentrations of 4-NP as well as rate constants 'k' were calculated. Figure 9b showed the dependence of rate constant 'k' on 4-NP concentration which provided a clear insight that 'k' value remarkably decreases with a higher concentration of 4-NP and summarized in Table S3. At the higher concentration of 4-NP, it was observed that 4-NP has more affinity to be adsorbed on Au NPs surface compared to BH_4^- ions that resulted in low available occupancy sites to BH_4^- on the Au NPs surface. As a result, low electron relay was observed among reactants that retarded reduction rate with a higher concentration of 4-NP. On the other hand, faster reaction was observed with higher rate constants when the concentration of 4-NP was low which may lead to less competition among BH_4^- and 4-NP.

The Effect of Concentration of $NaBH_4$

Similarly, the influence of concentration of $NaBH_4$ (2 to 10 mM) on the reduction of 4-NP was also determined by keeping the concentration of 4-NP (0.1 mM) and Au NPs (7 µL) as constant. ln(A_t/A_0) vs. time 't' was plotted for the different concentrations of $NaBH_4$ (Fig. 10a) also, rate constant 'k' values were calculated. It was observed that increase in concentration of $NaBH_4$ increases the rate constant 'k' values (Fig. 10b) which was tabulated in Table S3. With a low concentration of $NaBH_4$, only less

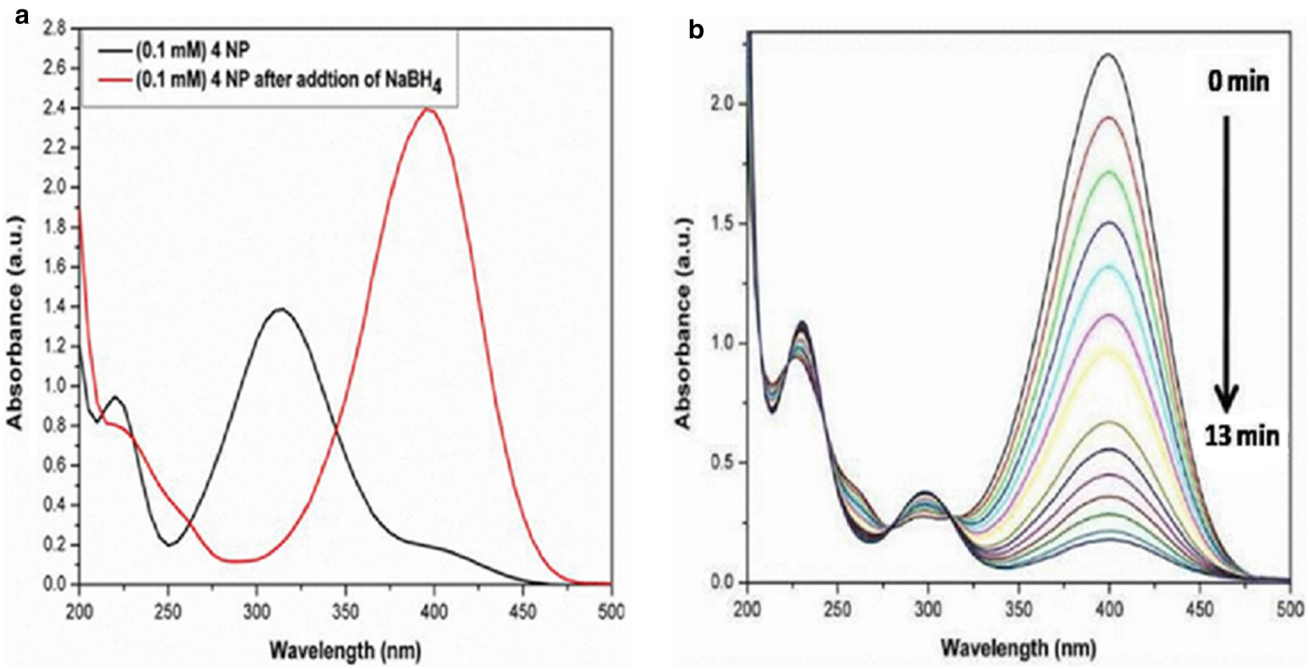

Fig. 7 **a** UV–Vis spectrum of comparison of 4-NP before and after addition of $NaBH_4$. **b** Kinetics of reduction of 4-NP (0.1 mM) with $NaBH_4$ (5 mM) catalyzed using Au NPs (7 μL)

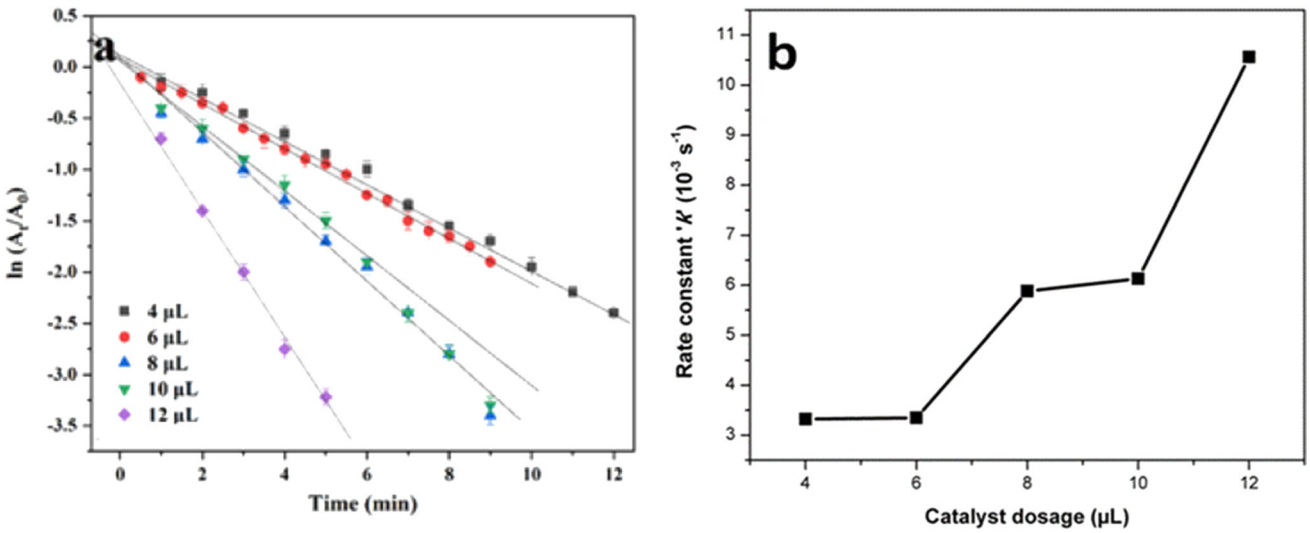

Fig. 8 **a** The plot of ln (A_t/A_0) vs time 't' for the reduction of 4-NP (0.1 mM) with various amount of Au NPs. **b** dependence of rate constant 'k' on the concentration of Au NPs catalysts

amount of BH_4^- ions have generated, which supplied fewer electrons to 4-NP that adsorbed on the Au NPs surface which slows down the electron relay process. Therefore, the reduction occurred gradually with lower rate constant 'k' values. Instantaneously, at a higher concentration of $NaBH_4$, rate constant 'k' values were observed to be increased implies that extra BH_4^- ions were available that supplies electrons toward 4-NP resulted in a fast increase in rate with quicker electron relay process.

Catalytic Activity of Different Sized Au NPs

Successfully, three different sized Au NPs (AmAu2, AmAu3 as well as AmAu4 NPs) were synthesized, so interested to examine the influence of particle size on the catalytic reduction of 4-NP. The progress as well as kinetic studies of 4-NP reduction in the presence of AmAu2, AmAu3, and AmAu4 nanoparticles also their corresponding plots ln (A_t/A_0) vs. time 't' were presented in Fig. 11. It was noted that the time required by AmAu4 nanoparticles

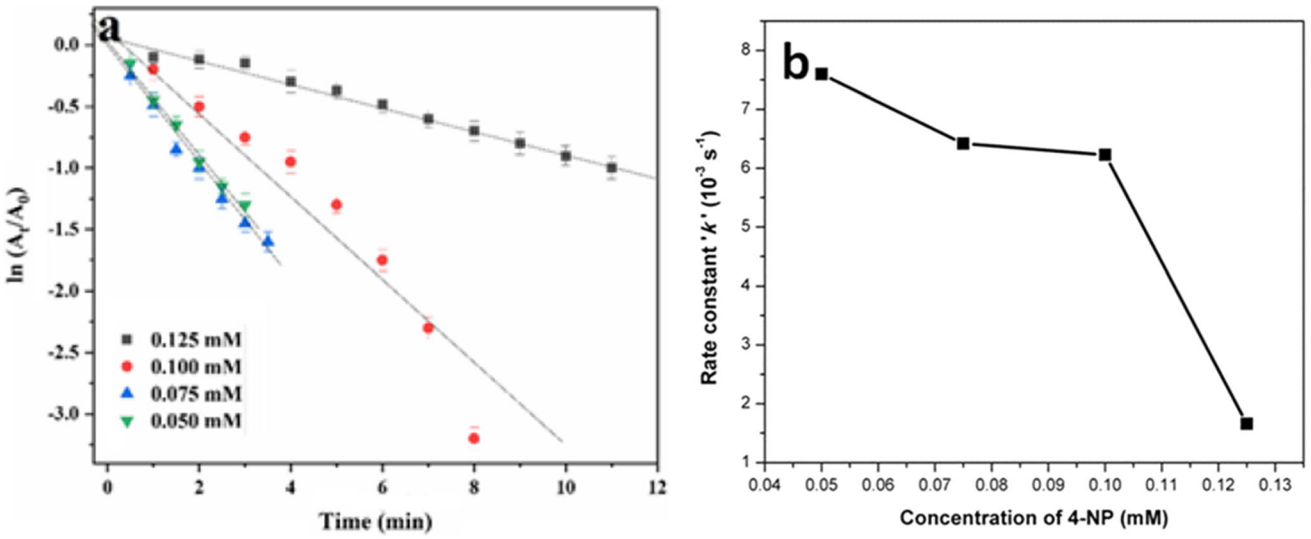

Fig. 9 **a** The Plot of ln (A_t/A_0) vs time 't' for Reduction of various concentration of 4-NP by 5 mM of $NaBH_4$. **b** Dependence of Rate Constant 'k' on the 4-NP concentration

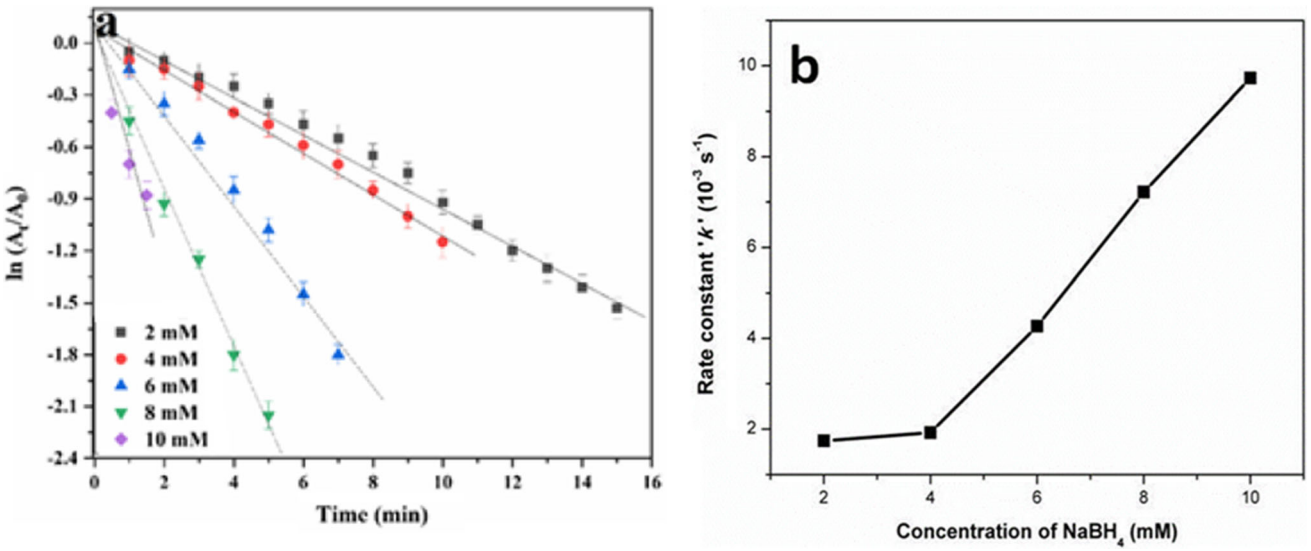

Fig. 10 **a** The Plot of ln (A_t/A_0) vs time 't' for Reduction of 4-NP (0.1 mM) with various concentration of $NaBH_4$. **b** Dependence of Rate Constant 'k' on the $NaBH_4$ concentration

for the complete reduction of 4-NP (0.1 mM) was almost 8 min, but AmAu2 as well as AmAu3 nanoparticles had taken 18 and 14 min respectively for reduction of equal quantity of 4-NP. The investigation indicated that the efficiency of the catalyst increases with smaller particle size of prepared Au NPs and the catalytic efficiency was found to be in the following order: AmAu4 > AmAu3 > AmAu2. The Au NPs with smaller sizes have a more surface-to-volume ratio which increases the active sites on the surface to execute better catalytic activity. The 'k' values observed for various sized Au NPs were summarized in Table S4.

Figure S2 represented the plausible mechanism for the catalytic efficiency of three different sized Au NPs on the reduction of 4-NP. From the systematic study, it was noted that rate constant 'k' value of AmAu4 was higher compared to AmAu3 as well as AmAu2 nanoparticles owing to less redox potential and smaller particle size that reduced the kinetic barrier, in turn, facilitated faster reduction of 4-NP through higher 'k' values [48]. Therefore, the entire results showed, the catalytic activities of the synthesized Au NPs were directly associated with the particle size. Moreover, the catalytic activity of prepared Au NPs were also compared with earlier reported synthesized Au NPs [33, 39, 40, 49] and observed that the found rate constant

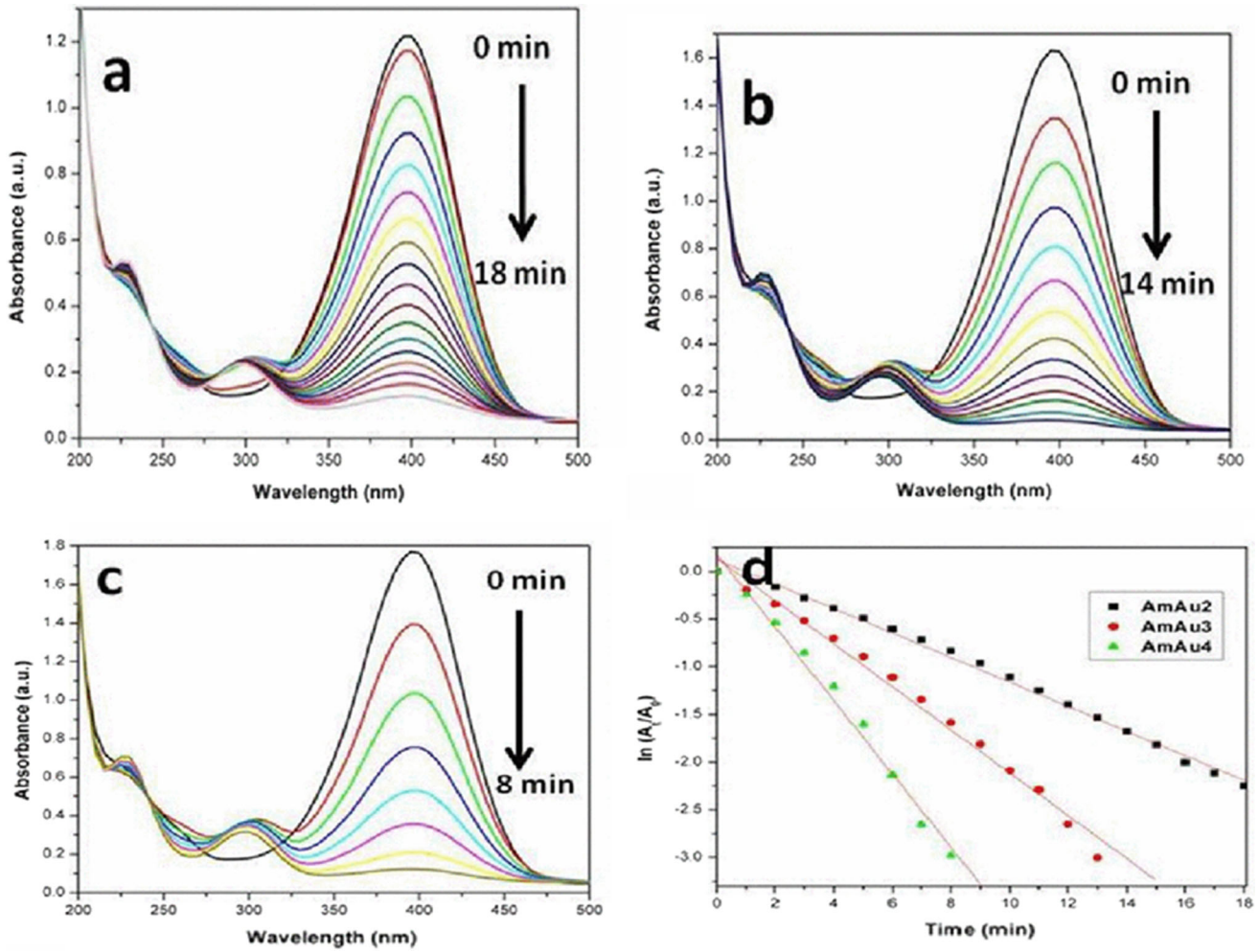

Fig. 11 The UV–Vis Absorption Spectra exhibiting the Reduction of 4-NP (0.1 mM) and 5 mM $NaBH_4$ Catalysed using 7 µL of **a** AmAu2, **b** AmAu3 and **c** AmAu4 Nanoparticles, **d** Corresponding Plots of $\ln(A_t/A_0)$ vs Time

'k' value was greater than the reported catalysts (Table 1). Therefore, it was emphasized that the synthesized Au NPs is a better catalyst for the reduction of 4-NP.

Size-Dependent Catalytic Studies of Different Sized Au NPs on the Reduction of 4-Nitrophenol

The catalytic efficiency of the AMB leaves extract mediated Au NPs were compared along with the influential parameters which were tabulated in Table S5. From Table S5, it was noted that the rate constant 'k' value of three different Au NPs was in the following order

Table 1 Comparison of Rate Constant 'k' for the Reduction of 4-NP by the Au NPs by different Green Reducing Agents

Catalyst	Calculated rate constant 'k' (10^{-3} s^{-1})	Reference
Actinodaphne madraspatna Bedd mediated Au NPs (This work)	6.44	Present work
Fagonia indica mediated Au NPs	3.4	[33]
Prunus domestica mediated Au NPs	5.1	[39]
Mussaenda glabrata mediated Au NPs	5.71	[40]
Garcinia combogia mediated Au NPs	2.23	[49]

AmAu4 > AmAu3 > AmAu2. AmAu4 NPs showed a fast catalytic reaction compared to other prepared Au NPs owing to their smaller particle size. By comparing 'k' values of synthesized Au NPs, it was found that the size and shape of the nanoparticles play a vital role in the catalytic reduction of 4-NP.

Conclusion

In summary, an eco-friendly method was adopted to synthesis Au NPs using aqueous leaves extract of *Actinodaphne madraspatna* Bedd. The average particle size of the prepared Au NPs was reduced from 80 to 20 nm, simply by increasing the AMB leaves extract concentration in synthesis protocol. Furthermore, the AMB leaves extract stabilized Au NPs demonstrated the significant catalytic efficiency towards the reduction of 4-NP through the electron relay process. The different influential parameters in the kinetic studies exhibited that rate constant 'k' increases by increase in Au NPs dosage as well as $NaBH_4$ concentration but get decreased with an increase in 4-NP concentration, which depicted the role of Au NPs as nanocatalyst. Besides, Au NPs synthesized with 4% concentration of AMB leaves extract exhibited higher catalytic activity towards the reduction of 4-NP and that is compared with other synthesized Au NPs owing to more surface-tovolume ratio because of their smaller particle size. The comparative catalytic study of all synthesized metal nanoparticles suggested that size-dependent redox potential as well as the availability of surface-to-volume ratio of metal nanoparticles were played an important role in the catalytic reduction. On the whole, the synthesized Au NPs were proved to be a suitable candidate for the environmental remediation of polluted water.

Supplementary Information The online version contains supplementary material available at https://doi.org/10.1007/s10876-021-02045-0.

Acknowledgements The authors are grateful to the "VIT SEED money Grant provided by VIT, Vellore to carry out this research work.

Declarations

Conflict of interest The authors have no conflict of interest.

References

1. L. S. Nair and C. T. Laurencine (2007). *J. Biomed. Nanotechnol.* **3**, 301–316.
2. J. You, L. Meng, and T. B. Song (2015). *Nat. Nanotechnol.* **11**, 1–8.
3. A. Manke, L. Wang, and Y. Rojanasakul (2013). *Biomed. Res. Int.* **2013**, 1–15.
4. S. M. Dizaj, F. Lotfipour, and M. Barzegar-Jalali (2014). *Mater. Sci. Eng. C.* **44**, 278–284.
5. N. H. A. Nguyen, M. S. A. Darwish, and I. Stibor (2017). *Nanoscale Res. Lett.* **12**, 571.
6. S. Deyev, G. Proshkina, A. Ryabova, F. Tavanti, M. C. Menziani, G. Eidelshtein, G. Avishai, and A. Kotlyar (2017). *Bioconj. Chem.* **28**, 2569–2574.
7. G. V. Khutale and A. Casey (2017). *Eur. J. Pharm. Biopharm.* **119**, 372–380.
8. V. K. Kumar and K. R. Gopidas (2010). *Chem. Asian J.* **5**, 887–896.
9. K. D. Lee, P. C. Nagajyothi, T. V. M. Sreekanth, and S. Park (2015). *J. Ind. Eng. Chem.* **26**, 67–72.
10. R. Karthik, M. Govindasamy, Shen-Ming. Chen, P. Yi-Hui Cheng, S. Muthukrishnan, and A. Elangovan. Padmavathy (2017). *J. Photochem. Photobiol. B* **170**, 164–172.
11. M. Stratakis and H. Garcia H, (2012). *Chem. Rev.* **112**, 4469–4506.
12. C. Jin, X. Cao, F. Lu, Z. Yang, and R. Yang (2014). *ACS Appl. Mater. Interfaces* **6**, 847–853.
13. T. C. Rojas, M. Multigner, J. M. De Fuente, J. C. Sa, A. Ferna, and A. Hernando (2004). *Phys. Rev. Lett* **93**, 4–7.
14. A. M. Funston, C. Novo, P. Mulvaney, and L. M. Liz-marza (2008). *Chem. Soc. Rev* **37**, 1792–1805.
15. Y. Kim, R. C. Johnson, and J. T. Hupp (2001). *Nano Lett.* **1**, 165–167.
16. R. Segura, J. Pizarro, K. Díaz, A. Placencio, F. Godoy, and E. Pino (2015). *Sens. Actuators B* **220**, 263–269.
17. T. Qian, C. Yu, S. Wu, and J. Shen (2013). *Colloids Surf. B* **112**, 310–314.
18. L. Dykmana and N. Khlebtsov (2012). *Chem. Soc. Rev* **41**, 2256–2282.
19. K. D. Lee, P. C. Nagajyothi, T. V. M. Sreekanth, and S. Park (2015). *J. Ind. Eng. Chem* **26**, 67–72.
20. P. Mohanpuria, N. K. Rana, and S. K. Yadav (2008). *J. Nanoparticle Res.* **10** (3), 507–517.
21. C. G. Yuan, C. Huo, S. Yu, and B. Gui (2017). *Physica E* **85**, 19–26.
22. C. Umamaheswari, A. Lakshmanan, and N. S. Nagarajan (2017). *J. Photochem. Photobiol. B* **178**, 33–39.
23. V. Reddy, R. S. Torati, S. Oh, and C. Kim (2013). *Ind. Eng. Chem. Res* **52** (2), 556–564.
24. S. Phukan, P. Bharali, A. K. Das, and M. H. Rashid (2016). *RSC Adv.* **6** (55), 49307–49316.
25. S. Francis, S. Joseph, E. P. Koshy, and B. Mathew (2017). *Environ. Sci. Pollut. Res. Int.* **24** (21), 17347–17357.
26. M. Nemanashi and R. Meijboom (2013). *J. Colloid Interface Sci.* **389** (1), 260–267.
27. X. Qiu, Q. Liu, M. Song, and C. Huang (2016). *J. Colloid Interface Sci.* **477**, 131–137.
28. Y. Li, Y. Cao, J. Xie, D. Jia, H. Qin, and Z. Liang (2015). *Catal. Commun.* **58**, 21–25.
29. I. V. Asharani and D. Thirumalai (2012). *J. Chin. Chem. Soc.* **59** (11), 1455–1460.
30. D. Badma Priya and I. V. Asharani (2017). *J. Clust. Sci.* **28** (4), 1837–1856.
31. D. Badma Priya and I. V. Asharani (2018). *IET Nanobiotechnol.* **12** (2), 116–126.
32. X. Dong, X. Ji, H. Wu, L. Zhao, J. Li, and W. Yang (2009). *J. Phys. Chem. C* **113** (16), 6573–6576.
33. A. Ahmad, Y. Wei, F. Syed, M. Imran, Z. U. H. Khan, K. Tahir, A. U. Khan, M. Raza, Q. Khan, and Q. Yuan (2015). *RSC Adv.* **5** (120), 99364–99377.
34. S. A. Aromal and D. Philip (2012). *Spectrochem. Acta A* **97**, 1–5.

35. I. V. Asharani and D. Saravanan (2013). *Asian J. Pharm. Clin. Res.* **6** (5), 114–118.
36. B. Suneetha, K. Prasad, B. Soumya, P. D. Nishantha, B. S. Kumar, and D. Rajaneekar (2014). *Res. Rev.* **6** (1), 1–4.
37. B. Suneetha, K. Prasad, P. D. Nishanthi, B. Soumya, and B. S. Kumar (2014). *Res. Rev.* **6** (4), 176–180.
38. M. Nasrollahzadeh, S. M. Sajadi, M. Maham, and A. Ehsani (2015). *RSC Adv.* **5** (4), 2562–2567.
39. P. Dauthal and M. Mukhopadhyay (2012). *Ind. Eng. Chem. Res* **51** (40), 13014–13020.
40. S. Francis, S. Joseph, E. P. Koshy, and B. Mathew (2017). *Environ. Sci. Pollut. Res.* **24** (21), 17347–17357.
41. S. K. Nune, N. Chanda, R. Shukla, K. Katti, R. R. Kulkarni, S. Thilakavathi, S. Mekapothula, R. Kannan, and K. V. Katti (2009). *J. Mater. Chem* **19** (19), 2912–2920.
42. W. Haiss, N. T. K. Tharh, J. Aveyard, and D. G. Fernig (2007). *Anal. Chem.* **79**, 4215–4221.
43. I. A. Wani, S. Khatoon, A. Ganguly, J. Ahmed, A. K. Ganguli, and T. Ahmad (2010). *Mater. Res. Bull.* **45**, 1033–1038.
44. Tokeer Ahmad, Irshad A. Wani, Jahangeer Ahmed, and Omar A. Al-Hartomy (2014). *Appl. Nanosci.* **4**, 491–498.
45. X. Q. Wu, X. W. Wu, Q. Huang, J. S. Shen, and H. W. Zhang (2015). *Appl. Surf. Sci.* **331**, 210–218.
46. M. Zhang, X. Lu, H. Y. Wang, X. Liu, Y. Qin, P. Zhang, and Z. X. Guo (2016). *RSC Adv.* **6** (42), 35945–35951.
47. X. Zhang, Y. Qu, W. Shen, J. Wang, H. Li, Z. Zhang, S. Li, and J. Zhou (2016). *Colloids Surf. A* **497**, 280–285.
48. Z. Zhang, C. Shao, Y. Sun, J. Mu, M. Zhang, P. Zhang, Z. Guo, P. Liang, C. Wang, and Y. Liu (2012). *J. Mater. Chem* **22** (4), 1387–1395.
49. A. Rajan, M. MeenaKumari, and D. Philip (2014). *Spectrochim. Acta A* **118**, 793–799.